PHYSICAL REVIEW B VOLUME 16, NUMBER 10 15 NOVEMBER 1977

Far-infrared dispersive-reflection measurements on NaCl, compared with calculations based on cubic and quartic anharmonicity. I. Room temperature*

J. E. Eldridge and P. R. Staal

Department of Physics, University of British Columbia, Vancouver, British Columbia V6T 1W5, Canada

(Received 7 June 1977)

Accurate dispersive-reflection measurements have been made on a large single crystal of NaCl at room temperature to yield the reflectance amplitude and phase between 25 and 500 cm^{-1} in the far infrared. These have been augmented with power-transmission measurements in those regions where the phase is small. From these the remaining optical properties have also been obtained, and specifically the damping spectrum of the zero-wave-vector TO resonance which is primarily responsible for the far-infrared optical properties. This has then been compared with calculations based on both cubic and quartic anharmonicity. The three-phonon damping arising from the quartic term was calculated as accurately as possible, with only one significant approximation involving the neglect of certain terms depending on the third potential derivative. The quartic-coupling coefficient for the rocksalt structure is derived and presented under this approximation. Assignments have been made of the phonons responsible for the major features in both the two- and three-phonon damping spectra, and the predominant role of the flat TO mode is observed in the latter case. The effect of the finite lifetimes of the two or three phonons to which the TO mode relaxes is also clearly seen in the higher-wave-number part of the damping spectrum, and so the calculated spectrum was corrected for this by convoluting with a Lorentzian of experimentally determined width. The resulting overall agreement between experiment and theory is excellent. Some possible causes of the small remaining discrepancies are mentioned. Future low-temperature measurements will be useful in this respect.

I. INTRODUCTION

The far-infrared optical properties, or dielectric response, of single-crystal alkali halides is a subject which has received considerable attention over the past 10 or 15 years. This was originally due to the relative simplicity of the materials, which allowed the underlying physical processes which are involved to be understood more easily. Recently, however, a new impetus has been given to the field because of the use of these materials as windows for high-powered lasers. The residual absorption in the multiphonon region well above the main reststrahlen band is of considerable importance. In the reststrahlen region itself, considerable advances have been made in the accuracy of both the theoretical calculations and the experimental results, so that the agreement between the two has been steadily improving. Discrepancies have, however, remained and their cause, as well as the relative importance of certain theoretical approximations which have invariably been made, have not been clear. It is the purpose of this paper to present very accurate experimental data on sodium chloride together with the corresponding calculated spectra, which are considerably improved over those previously published, in order to show just how well the two now agree, and to comment on the probable cause of the very small remaining discrepancies.

For a long time, the experimental optical properties were determined from a Kramers-Kronig analysis of the power reflectivity. Sometimes these results would be supplemented with absorption coefficients from transmission data taken in the wings of the reststrahlen band where the absorption is not too high for bulk samples. Kramers-Kronig analyses are poor in those portions of the wings where the imaginary function is much less than the real function, and consequently both the magnitude and structure is lost, as has been demonstrated by one of us.[1] Furthermore, considerable structure around the longitudinal-optical (LO) phonon region is lost since the power reflectivity is so small there.[2] Metal-backed thin films have recently been used[3] to investigate predominantly the reststrahlen band and in particular the LO region, but the information gained is incomplete and surface effects can be important. Bell and co-workers[2,4,5] showed that considerable advantages were gained by the technique of dispersive-reflection, or asymmetric, Fourier spectroscopy, in which the sample either replaces the mirror in one of the arms of a Michelson interferometer, or is merely inserted into the beam in one of the interferometer arms for transmission measurements. Both the real and imaginary properties are measured simultaneously and since the amplitude reflectivity is measured rather than the power, then the structure around the LO region is easily obtained. A few groups[6-8] are now capable of making such asymmetric measurements,

and some of these have initially looked at alkali halides in order to evaluate their spectrometer performance. We have therefore converted our Michelson FS720 to operate in the dispersive-reflection mode but have avoided most of the phase errors which can be incurred in this technique by suitable improvements in design.[9]

Many papers[2,5,10-19] have appeared on the theory and calculations of the far-infrared properties of alkali halides, only a selected few of which are referenced here. They have all involved at least the contribution of cubic anharmonicity to the damping of the zero-wave-vector ($\vec{k}=0$) transverse-optical (TO) resonant mode of the crystal. By this mechanism, any infrared photon excites the TO mode off resonance, which then decays by either creating two phonons (*summation* processes) or creating one and destroying another (*difference* processes), energy and effectively zero momentum being conserved overall. This contribution has been calculated with various degrees of approximation, artificial fitting, and resolution. Earlier calculations used lattice-dynamical theories to generate the necessary input data for the calculation, whereas more recently shell-model data, fitted to inelastic neutron-scattering measurements of phonon-dispersion curves, have been employed. The contribution from quartic anharmonicity has sometimes been calculated, but this has usually involved considerable and sometimes unrealistic approximations. Occasionally the contribution from the second-order dipole moment has been added, but this has been shown to be small[11] and evidence of its neglect in the multiphonon wings away from the resonance, where it would become most noticeable, has not yet been forthcoming. In all of the calculations, the corresponding contributions to the energy shift of the TO mode has been calculated, sometimes together with frequency-independent shifts.

In particular, one of us has calculated the optical properties, based on cubic anharmonicity only, of LiF,[20,1] KI,[21] and the cubic-structured CsI.[22,23] For these materials, the *summation* and *difference* contributions were calculated separately; the cubic-coupling coefficient was analyzed to give the allowed and forbidden two-phonon combinations along the major symmetry directions; and the TO damping was analysed, with the aid of the phonon dispersion data and a set of criteria based on the cubic-coupling coefficient, to identify the combining phonons responsible for the major features in the damping spectra. In all of the materials shell-model data were found to be essential for really good agreement[1,23] in the position of features. In the case of LiF, which contains 7.5 at.% of Li^6 a further contribution to the damping, due to the isotope-induced one-phonon processes, was found to be the major damping mechanism of the TO mode at the resonance wave number ($\bar{\nu}_0$) at low temperatures.[24] The potential derivatives used in the calculation of the cubic coupling coefficient were calculated from first principles, with various approximate methods used to include the effect of other-than-nearest neighbors. No fitting or scaling was done. The major discrepancies in the calculated spectra were the obvious need for contributions from quartic anharmonicity both at $\bar{\nu}_0$ and beyond the two-phonon limit, and the excessive sharpness of the calculated two-phonon features.

It is the purpose of this paper to deal with the last two points mentioned above, and to compare the resulting calculated spectra with experimental data measured accurately throughout the far-infrared at room temperature. Dispersive-reflection spectroscopy at liquid-helium temperatures is not easily performed, and we are presently involved in the construction of the necessary cryogenic system. The results obtained will be presented in a later publication.

II. EXPERIMENTAL

Our commercial RIIC FS720 Fourier spectrometer has been converted to operate in the asymmetric mode, whereby the sample replaces the stationary mirror. The sample was a 76-mm-diam 8-mm-thick laser window from Harshaw Chemical Co. which had been flat polished to within 0.3 μm over our working area. An iris diaphragm limited the working area to a diameter of 55 mm. The thickness was sufficient to reduce any reflected intensity from the back face to a negligible quantity. In order to avoid the phase errors obtained when the sample is physically replaced by the required reference mirror, the sample was aluminized in the manner shown in Fig. 1, and the switching mask, also shown, was rotated in front of it at each step of the moving-mirror micrometer drive. Dual interferograms of sample and reference were

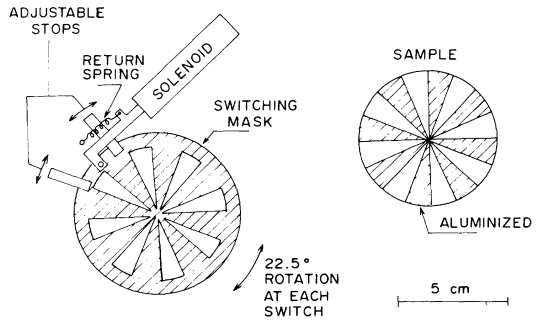

FIG. 1. Aluminized sample and the eight-section switching mask.

therefore obtained in a single run. This technique of switching between the sample and reference at each step eliminates phase errors due to micrometer-drive backlash, component-performance drift, and path-length variation due to thermal drift. The mask design allows easy alignment and eliminates extra runs needed to correct for beam nonuniformity. A 4-K bolometer was used as a detector providing the sensitivity and short time constant needed in these measurements. Further details of the method and instrument modifications have already been reported.[9]

When aluminized portions of the sample are used as a reference, corrections must be made due to the fact that the aluminum is not perfectly reflecting, nor is the phase change exactly π. For a parallel metal slab of thickness d, in which multiple reflections can occur, illuminated by radiation of wavelength λ at normal incidence, the ratio of the reflected field to the incident field is given by[25]

$$\frac{E_r}{E_i} = \frac{(e^{i\alpha}e^{\beta} - e^{-i\alpha}e^{-\beta})(1-n^2+k^2+2ink)}{e^{i\alpha}e^{\beta}(1+n-ik)^2 - e^{-i\alpha}e^{-\beta}(1-n+ik)^2}, \quad (1)$$

where

$$\alpha = 2\pi nd/\lambda, \quad \beta = 2\pi kd/\lambda, \quad (2)$$

and n and k are the refractive index and extinction coefficient of the metal. These in turn were calculated from the Drude theory in which

$$n^2 - k^2 = 1 - 4\pi\sigma_0\tau/(1+\omega^2\tau^2) \quad (3)$$

and

$$nk = 2\pi\sigma_0/\omega(1+\omega^2\tau^2), \quad (4)$$

where σ_0 is the dc conductivity, taken as 3.18×10^{17} sec^{-1} for aluminum, and τ is the scattering time taken as 0.801×10^{-14} sec. The thickness d was given by a digital thickness monitor to be 700 Å ± 5%. Analysis of Eq. (1) gives the reflectance amplitude and phase as a function of wave number, which may be seen in Fig. 2. Together with the phase calculated above, there is another phase difference, also shown in Fig. 2, due to the optical path difference of $2d$ between the sample and reference beam.

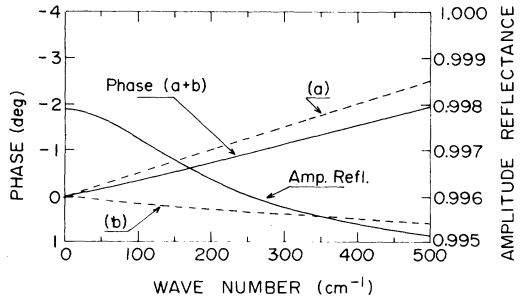

FIG. 2. Reflectance amplitude and phase difference from π of a 700-Å-thick layer of aluminum. The phase difference (a) is due to the optical path difference while (b) is due to the skin depth and finite thickness of the aluminum.

The reflection results were the average of four runs, each of 50 min duration. The resolution obtained, after apodisation, was 2 cm^{-1} (the maximum path difference was 0.5 cm). The reflectivity was sufficiently strong to give good amplitude results from 25 to 500 cm^{-1}, whereas the phase became very small below 110 cm^{-1} and above 340 cm^{-1}. The phase in these regions was obtained indirectly therefore from transmission measurements on cleaved crystals, varying in thickness from 0.03 to 0.2 cm, which yielded directly the absorption coefficient. These data will be presented in Sec. IV together with the calculated spectra.

III. THEORY AND CALCULATIONS OF THE COMPLEX PHASE SHIFT

Our starting point for the calculation of the optical properties is the complex dielectric constant given in Eq. (1) of Ref. 22, and reproduced here for convenience

$$\hat{\epsilon} = \epsilon' + i\epsilon'' = \epsilon_\infty + \frac{e^{*2}(M^+ + M^-)}{\pi v c^2 M^+ M^- \{\bar{\nu}_0^2 - \bar{\nu}^2 + 2\bar{\nu}_0[\Delta'(0,j_0;\bar{\nu}) - i\Gamma(0,j_0;\bar{\nu})]\}}, \quad (5)$$

where M^+ and M^- are the masses of the Na^+ and Cl^- ions, v is the volume of the unit cell, $\bar{\nu}_0$ (cm^{-1}) is the observed wave number of the TO lattice resonance, which has a wave vector $\vec{k}$ effectively equal to zero and branch index j_0, and e^* is the macroscopic effective charge associated with the TO mode. $\Delta'(0,j_0;\bar{\nu})$ and $\Gamma(0,j_0;\bar{\nu})$ are the real and imaginary parts of the phase shift (or Hermitian and anti-Hermitian parts of the proper self-energy matrix), and represent the wave-number shift and damping (both in wave numbers), respectively, of the TO mode, when excited by radiation of wave number $\bar{\nu}$. The calculation of the magnitude and structure of the optical properties is predominantly a matter of calculating the damping $\Gamma(0,j_0;\bar{\nu})$.

TABLE I. Constants used in the calculations (290 K).

Observed TO resonance wave number [a]	$\bar{\nu}_0$ (cm^{-1})	164
Static dielectric constant [a]	ϵ_0	5.90
High-frequency dielectric constant [a]	ϵ_∞	2.33
Madelung constant	α	1.747 56
Nearest-neighbor distance [b]	r_0 (10^{-8} cm)	2.813 8
Ionic masses	M^+ (amu)	22.989 8
	M^- (amu)	35.453
Compressibility [c]	β (10^{-12}/bar)	4.17
Repulsive overlap potential parameters	C (10^{-10} erg)	16.64
	ρ (10^{-8} cm)	0.323
Fourth potential derivative	$r_0\phi''''(r_0)$ (10^{12} erg cm^{-3})	62.03
Third potential derivative	$\phi'''(r_0)$ (10^{12} erg cm^{-3})	−5.926
Second potential derivative	$\phi''(r_0)/r_0$ (10^{12} erg cm^{-3})	0.198
First potential derivative	$\phi'(r_0)/r_0^2$ (10^{12} erg cm^{-3})	0.261

[a] See Ref. 26. [b] See Ref. 27. [c] See Ref. 28.

A. Two-phonon damping resulting from cubic anharmonicity

These two-phonon processes constitute the major damping mechanism in these materials around the resonance, as has been well demonstrated. The damping (in wave numbers) is given by [Eq. (3) of Ref. 22]

$$\Gamma(0,j_0;\bar{\nu}) = \frac{9}{2\pi c^2\hbar^2}\sum_{\vec{k}j_1}\sum_{-\vec{k}j_2}|V^{(3)}(0,j_0;\vec{k},j_1;-\vec{k},j_2)|^2 \times S(\bar{\nu}) \ (\mathrm{cm}^{-1}) \qquad (6)$$

where $V^{(3)}$ is the cubic-coupling coefficient (which has been previously given in several places[20,1]), and $S(\bar{\nu})$ contains the temperature dependence through the creation and annihilation operators, and conserves energy [Eqs. (4) and (5) in Ref. 22].

The various parameters used to calculate the damping, abbreviated to $\Gamma(\bar{\nu})$, may be found in Table I. The potential used was of the usual form

$$\phi(r_0) = -\alpha e^2/r_0 + 6Ce^{-r_0/\rho}, \qquad (7)$$

where only nearest neighbors have been considered in the repulsive term above, since this has been found to give good results for[1] LiF and[21] KI, whereas second-nearest neighbors were needed for the CsI structure.[22] The usual Madelung constant has also been used rather than the modified α'' from Ref. 1 since the latter has been shown to be incorrect due to the zero anharmonic coupling contribution from like ions.

The lattice-dynamical input data were generated by a shell model using the eleven-parameter model II of Schmunk and Winder,[29] which was fitted to inelastic-neutron-scattering data. The dispersion curves given by the model are shown in Fig. 3. A grid density of 108 000 points per zone was used for the two-phonon $\Gamma(\bar{\nu})$ computations.

The results may be seen in Fig. 4 together with

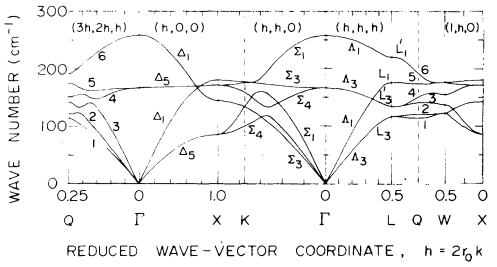

FIG. 3. Frequency dispersion curves along the major symmetry directions, as well as some other regions, generated by the eleven-parameter shell model of Schmunk and Winder (Ref. 29) for NaCl at room temperature. (The two Δ_1 curves do not actually cross but approach each other with a separation of 0.4 cm^{-1}.)

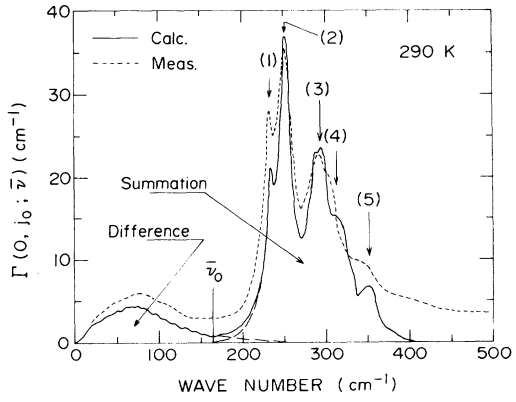

FIG. 4. Measured damping spectrum of the TO resonance in NaCl at 290 K with 2-cm^{-1} (wave-number) resolution, together with the calculated two-phonon contribution to that damping with equal resolution. The large-dashed lines show the separation contributions from the *difference* and *summation* processes.

the experimental spectrum obtained from the measured optical properties, which will be shown in Sec. IV. Both the calculated *summation* and *difference* damping, as well as the total, have been indicated.

Only five prominent features occur in the calculated spectrum and these have been labeled in Fig. 4. They are all summation features. Criteria for establishing the combination strength of any two phonons have already been given,[20] as well as the considerations needed to determine which phonon pairs are responsible for the limits of the damping from the two kinds of processes.[21] It has been seen, with both KI and LiF, that few of the strong features are due to phonon pairs at the highest-symmetry points, and indeed only at L are they possible. The next most favorable region is usually halfway along Γ to K where $\Sigma\Sigma$ pairs are found, but then the remainder come from low-symmetry regions in the center of the zone. The situation is found to be similar here for NaCl, except that combinations from branches running from Γ to Q are even more predominant. While several regions contribute at the wave number (234 cm^{-1}) of feature (1) in Fig. 4, the peak itself is due entirely to the sum of the two branches labeled 1 and 2 in Fig. 3 at Q. It may seem strange at first that a strong combination would be obtained between two acoustic modes, since in the criteria already mentioned[20] it was noted that the intensity would be enhanced if one of the eigenvectors were of opposite sign to the other three, giving strong coupling between "normal" acoustical and optical modes. These two branches at Q, however, satisfy very strongly all the remaining criteria. They have equal and opposite slopes, being nearly flat (see from L to W in Fig. 3). The $\sin(2\pi r_0 k_\alpha)$ term in the coupling coefficient is large for all three wave-vector components. All modes at Q have eigenvector components in the same direction, and finally the multiplicity of 24 at Q is the highest possible for any zone-boundary point. Feature (2) at 251 cm^{-1} is due to L_3L_3', which has been the strongest in all of the compounds investigated so far, plus $\Sigma_4(\mathrm{TA})\Sigma_4(\mathrm{TO})$. The calculated feature (3) is actually a pair of combinations, branches 3 and 4 near Q, at 286 cm^{-1} and 2 and 5 near Q, at 295 cm^{-1}. Experimentally these do not resolve. Feature (4) is from $\Sigma_4(\mathrm{TA})\Sigma_1(\mathrm{LO})$ and branches 1 plus 6, and 4 plus 5, two-thirds of the way from Γ to Q. The last feature, (5) is partially $\Sigma_1\Sigma_1$ and partially from a region near W.

B. Isotope-induced one-phonon damping

In LiF this damping was found to be considerable at $\bar{\nu}_0$ at room temperature.[1] In natural NaCl the chlorine is ^{35}Cl (75%) and ^{37}Cl (24%) and the one-phonon damping spectrum due to this has therefore been calculated. It is found, however, to be negligible at room temperature [$\Gamma(\bar{\nu})$ at $\bar{\nu}_0 \sim 0.05$ cm^{-1}, approximately 1% of $\Gamma(\bar{\nu})$ measured]. It will probably become important at low temperatures, and so the spectrum will be presented in the second part of this paper which will deal with those results.

C. Three-phonon damping resulting from quartic anharmonicity

It is clear from Fig. 4 that the two-phonon damping is insufficient around $\bar{\nu}_0$ and that the damping beyond 400 cm^{-1} must come from higher-order terms. The simplest and most important three-phonon contribution is given by

$$\Gamma_{3\text{-ph}}(0,j_0;\bar{\nu}) = \frac{48}{2\pi c^2\hbar^2} \sum_{\substack{\vec{k}_1 \\ \pm j_1}} \sum_{\substack{\vec{k}_2 \\ \pm j_2}} \sum_{\substack{\vec{k}_3 \\ \pm j_3}} |V^{(4)}(0,j_0;\vec{k}_1,j_1;\vec{k}_2,j_2;\vec{k}_3,j_3)|^2 S(\bar{\nu}) \quad (\mathrm{cm}^{-1}), \tag{8}$$

where

$$S(\bar{\nu}) = [(n_1+1)(n_2+1)(n_3+1) - n_1n_2n_3] \times \delta(\bar{\nu} - \bar{\nu}_1 - \bar{\nu}_2 - \bar{\nu}_3) \tag{9}$$

for a *summation* case, and

$$S(\bar{\nu}) = [(n_1+1)(n_2+1)n_3 - n_1n_2(n_3+1)] \times \delta(\bar{\nu} - \bar{\nu}_1 - \bar{\nu}_2 + \bar{\nu}_3) \tag{10}$$

for a *difference* case in which for example the third phonon is destroyed.

The occupation number n is given by

$$n(\vec{k},j) = [\exp(h\bar{\nu}(\vec{k},j)c/k_BT) - 1]^{-1}. \tag{11}$$

The notation of Wallis *et al.*[16] has been used, in which the sum over $\pm j_i$ indicates a sum over $\pm\bar{\nu}_i$, and of course the appropriate expression for $S(\bar{\nu})$ must be used in each case.

Only a few authors have calculated this contribution, and in each case certain approximations have been made to reduce the computing time and complexity. These have included working in the high-

temperature limit, ignoring the $\vec{k}$ dependence of $V^{(4)}$ and by treating $V^{(4)}$ as a constant. We felt that it would be worthwhile to calculate this three-phonon damping as accurately as possible, since it is the predominant term around $\bar{\nu}_0$ at room temperature, and just above the two-phonon limit at most temperatures. There is also evidence of broad structure in this last region for certain compounds.[30] Consequently we have made none of the above approximations.

The general expression for the V coefficients is given in Eq. (2.2) of Ref. 16. We have evaluated $V^{(4)}$ from this for the rocksalt structure in a manner similar to that outlined in Ref. 22 for $V^{(3)}$ for CsI. This involved considering nearest neighbors only (which is the usual approximation and a fairly good one since the second-nearest neighbors are like ions and do not contribute at all), and also that the incident photon is polarized with the electric field along the x axis. When one converts the fourth Cartesian derivative of the potential $\phi_{\alpha_1\alpha_2\alpha_3\alpha_4}$ to radial derivatives, and restricts α_1 to x, then the result for the neighbors in the x direction may be seen in Table II. Here $\phi''(r_0)$ and $\phi'(r_0)$ have been neglected since they are so small (see Table I). Only ϕ_{xxxx} contains $\phi''''(r_0)$ which is easily the largest term (see Table I again). However $6\phi'''(r_0)/r_0$ is just over half of $\phi''''(r_0)$ and one would not expect to neglect it. The calculation of any of the general terms $\phi_{x\alpha_2\alpha_3\alpha_4}$, however, takes at least N/N_i as much computing time as the calculation of ϕ_{xxxx}, where N is the number of wave-vector points in the first Brillouin zone and N_i is the number of irreducible points in the same zone.

TABLE II. Force-constant tensor for the two nearest neighbors lying along the polarization direction x of the incident photon.

$$\begin{bmatrix} \phi_{xxxx} & \phi_{xxxy} & \phi_{xxxz} \\ \phi_{xxyx} & \phi_{xxyy} & \phi_{xxyz} \\ \phi_{xxzx} & \phi_{xxzy} & \phi_{xxzz} \\ \phi_{xyxx} & \phi_{xyxy} & \phi_{xyxz} \\ \phi_{xyyx} & \phi_{xyyy} & \phi_{xyyz} \\ \phi_{xyzx} & \phi_{xyzy} & \phi_{xyzz} \\ \phi_{xzxx} & \phi_{xzxy} & \phi_{xzxz} \\ \phi_{xzyx} & \phi_{xzyy} & \phi_{xzyz} \\ \phi_{xzzx} & \phi_{xzzy} & \phi_{xzzz} \end{bmatrix} = \begin{bmatrix} \eta & 0 & 0 \\ 0 & \tau & 0 \\ 0 & 0 & \tau \\ 0 & \tau & 0 \\ \tau & 0 & 0 \\ 0 & 0 & 0 \\ 0 & 0 & \tau \\ 0 & 0 & 0 \\ \tau & 0 & 0 \end{bmatrix}$$

$$\eta = \phi''''(r_0) - (6/r_0)\phi'''(r_0)$$

$$\tau = (1/r_0)\phi'''(r_0)$$

In our case we chose an N_i of 27 which gave N equal to 499, not counting the origin. The central-processing-unit time needed to compute the full three-phonon spectrum using just ϕ_{xxxx} was 24 min. It can be seen therefore that this predominant term is the only one which can be calculated exactly, but that the six other nonzero terms in Table II will cancel fairly well with the $\phi'''(r_0)$ term in ϕ_{xxxx}. The final expression therefore contained only $\phi''''(r_0)$. [Neighbors lying along the y and z directions contribute no term with $\phi''''(r_0)$ and only three with $\phi'''(r_0)$, which have also necessarily been neglected.] The expression derived is

$$V^{(4)}(0,j_0;\vec{k}_1,j_1;\vec{k}_2,j_2;\vec{k}_3,j_3) = \frac{\hbar^2}{48N}\left(\frac{1}{(2\pi c)^4\bar{\nu}_0\bar{\nu}_1\bar{\nu}_2\bar{\nu}_3}\right)^{1/2}\phi''''(r_0)\left(\frac{M^+ + M^-}{M^+M^-}\right)^{1/2}$$
$$\times[(A^+_{x1}A^+_{x2}A^+_{x3} - A^-_{x1}A^-_{x2}A^-_{x3}) + (A^+_{x1}A^-_{x2}A^-_{x3} - A^-_{x1}A^+_{x2}A^+_{x3})\cos(2\pi r_0 k_{1x})$$
$$+ (A^-_{x1}A^+_{x2}A^-_{x3} - A^+_{x1}A^-_{x2}A^+_{x3})\cos(2\pi r_0 k_{2x}) + (A^-_{x1}A^-_{x2}A^+_{x3} - A^+_{x1}A^+_{x2}A^-_{x3})\cos(2\pi r_0 k_{3x})]$$
$$\times\Delta(\vec{k}_1+\vec{k}_2+\vec{k}_3), \tag{12}$$

where

$$A^+_{x1} = m^+_x(\vec{k}_1 j_1)/(M^+)^{1/2}, \tag{13}$$

in which $m^+_x(\vec{k}_1 j_1)$ is the x component of the eigenvector for the Na^+ ion when disturbed by the mode $\vec{k}_1 j_1$, and k_{1x} is the x component of the wave vector of the first phonon. The Δ function conserves momentum and has the property that

$$\Delta(\vec{k}_1+\vec{k}_2+\vec{k}_3) = \begin{cases} 1 & \text{if } \vec{k}_1+\vec{k}_2+\vec{k}_3 = 0 \text{ or } \vec{G} \\ & \text{(umklapp process)}, \\ 0 & \text{otherwise}. \end{cases} \tag{14}$$

$\vec{G}$ is a reciprocal-lattice vector.

The result may be seen in Fig. 5 where the *summation* and *difference* processes have been drawn separately where they overlap. In this regard, *difference* may be taken to mean the destruction of only one phonon since the damping due to processes involving the destruction of two phonons is so small it is hardly visible on the graph. The form and magnitude of Fig. 5 is similar to that obtained by Bruce[14] for KBr, who it is felt used a comparable expression for $V^{(4)}$ (see for example Ref. 31) although this is not clear. It is interesting to assign the phonons responsible for the structure seen

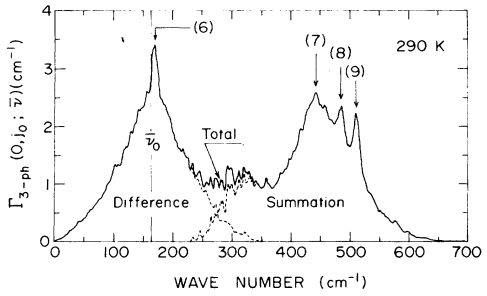

FIG. 5. Calculated three-phonon damping of the TO resonance in NaCl at 290 K with 2-cm^{-1} resolution. The dashed lines show the separate contributions of the *summation* and *difference* processes.

in the spectrum, and the four main features have been indicated. (The structure around 300 cm^{-1} is mainly grid noise resulting from the calculation.) The predominant phonon involved in all of the features is the TO mode which is so flat across most of the zone (see Fig. 3). It has an average wave number of 170 cm^{-1}, and so peak (6) at 170 cm^{-1} is the creation of two and the destruction of one, while peak (9) at 510 cm^{-1} is the creation of three. Peak (8) at 485 cm^{-1} is the creation of two TO modes together with a mode around 140 cm^{-1} (e.g., between X and K and X and L), while peak (7) at 444 cm^{-1} is two TO modes plus an acoustical mode around 100 cm^{-1}. Also contributing here is the combination of TO plus two modes around 140 cm^{-1}. One can see by inspection of $V^{(4)}$ [Eq. (12)] that once again the coupling is enhanced if one or all three of the modes have an optical nature, i.e., the eigenvectors are of opposite sign. Note, however, that the eigenvectors for the longitudinal-optical mode between Γ and X, for example, change halfway across the zone to having the same sign, in order to preserve the optical nature of the mode, in which the nearest neighbors are displaced in opposite directions. This is of course accompanied by a similar change in the longitudinal-acoustical mode eigenvectors, so that the two-phonon enhancement remains strong. This enhancement in the three-phonon case is not strongly evident in the present spectrum for NaCl, since there is no energy gap in the phonon spectrum so that many modes cross and change nature throughout the zone. Of greatest importance is the high density of states of the TO mode, as already mentioned. Subsequent to Ref. 20 in which the two-phonon enhancement was pointed out, Duthler and Sparks[32] reported it as a quasiselection rule. Recently, Duthler[33] has extended this rule to multiphonon processes and theoretically demonstrated in a much more instructive manner the enhancement mentioned above, namely, that obtained when an odd number of optical phonons is involved. In particular a distinction is drawn between materials without a gap, such as NaCl and LiF, and those with a gap such as NaI and KI in which the modes tend to maintain a constant nature across the zone. In these materials then, the combination of two optic modes and an acoustic mode is obviously unfavorable, and, accentuated by the gap itself, the feature due to the sum of three optic modes stands out clearly from the rest of the spectrum. This feature has been experimentally observed.[30] We have calculated the three-phonon spectrum for KI at 300 and 80 K and demonstrated this behavior in agreement with experiment. This is being published as a comment concurrently.[34]

Two further points may be mentioned. The first is the relative magnitude of the *difference* and *summation* damping in Fig. 5 compared with the two-phonon case. This is to be expected since there are *three* times as many ways to destroy one TO mode and create two, as there are ways of creating three TO modes. The second is the wave number at which the *summation* processes start, which as expected[21] is approximately three times the wave number, 80 cm^{-1}, of the lowest acoustical modes halfway across the zone.

D. Damping of the "final-state" phonons

Figure 6 shows the effect of adding in the three-phonon contribution. There is an improvement but there remains an obvious fault in the computed spectrum, namely the excessive sharpness of some of the features (e.g., at $\bar{\nu}_0$ and 350 cm^{-1}). Previously[1] this was attributed to the neglect of further neighbors in the coupling coefficients, but since like ions do not contribute at all, this is clearly not the main reason. The lifetimes of the two or three phonons themselves, which are involved in the TO relaxation, have to be consid-

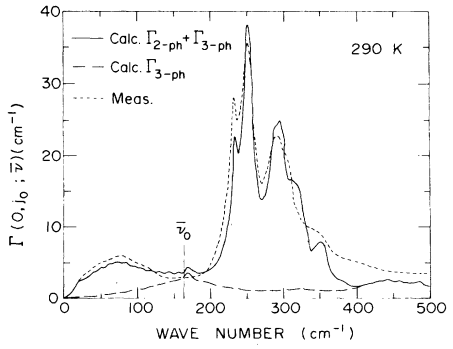

FIG. 6. Measured damping spectrum of the TO resonance in NaCl at 290 K with 2-cm^{-1} (wave-number) resolution, together with the two- and three-phonon contributions to that damping, with equal resolution.

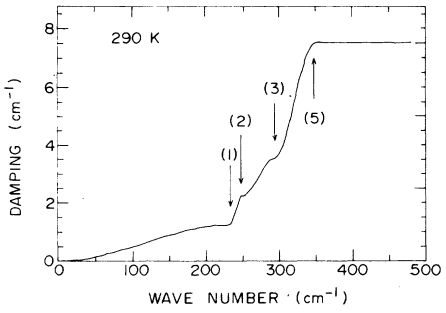

FIG. 7. Damping of the "final-state" two phonons, as a function of wave number. The damping was experimentally determined at the four features indicated above and in Fig. 4. A cubic polynomial was used to join the four points above, with zero slope at each point. The calculated two-phonon spectrum was convoluted with a Lorentzian of the varying half-width at half-maximum given above.

ered.[33,14] Fischer[35] has done this in a self-consistent manner. We, on the other hand, have obtained the widths of the four sharp features in Fig. 4 from the measured spectrum and have then convoluted our calculated two-phonon spectrum with a Lorentzian function of varying width. Figure 7 shows the half-width at half-maximum of the Lorentzian as a function of wave number. The values obtained are reasonable when one considers which phonons are involved, what their widths are likely to be (see for example Ref. 35) and that the sum of the individual widths has to be used. Due to the predominant role of the high-$\vec{k}$ TO phonons in the three-phonon contribution, the damping of the three-phonon states is a little easier to estimate. The damping of the zero-$\vec{k}$ TO mode is what has been measured in this experiment, and may be seen to be about 3 cm^{-1} at $\bar{\nu}_0$ in Fig. 4. This would indicate that a Lorentzian with a constant half-width of 9 cm^{-1} should be used to convolute the spectrum of Fig. 5, and the result may be seen in Fig. 8. The previous *summation* features of Fig. 5 are now seen to be unresolved.

The final result is seen in Fig. 9, where the

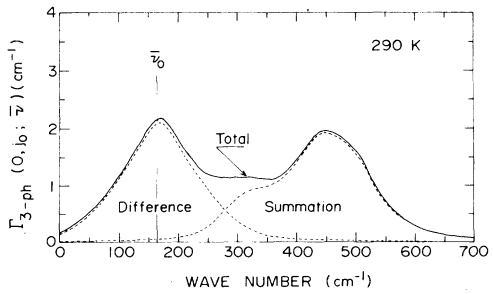

FIG. 8. Calculated three-phonon damping of the TO resonance in NaCl at 290 K after convolution with a Lorentzian of 9 cm^{-1} half-width at half-maximum.

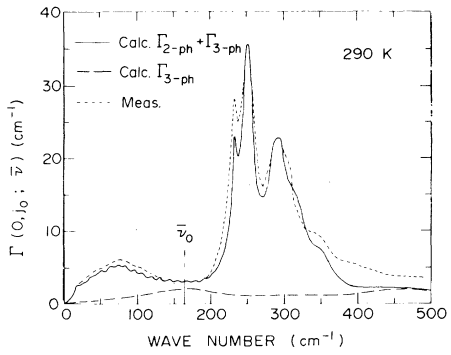

FIG. 9. Measured damping spectrum of the TO resonance in NaCl at 290 K with 2-cm^{-1} (wave-number) resolution, together with the calculated two- and three-phonon contributions to that damping, after correcting for the lifetime of these two and three phonons.

overall agreement is very good. In particular the agreement at $\bar{\nu}_0$ is excellent and shows the proportion of two- to three-phonon damping responsible (both of the difference type). The remaining discrepancies may be due to one or more of the following: errors in the neutron data, specifically the eigenvectors; neglect of further neighbors in the coupling; neglect of the second-order dipole moment about 350 cm^{-1}; incorrect three-phonon damping above 350 cm^{-1}; neglect of multiphonon damping above 350 cm^{-1}; incorrect width of "final-state" phonons above 350 cm^{-1}; neglect of other contributions to the damping from different diagrams (see Bruce[14]). Of these it is felt that the multiphonon processes above 350 cm^{-1} are the most important, and specifically at 400 cm^{-1} a strong broad contribution from the four-phonon process involving the creation of three TO modes (510 cm^{-1}) and the destruction of an acoustical mode (110 cm^{-1}) is expected. This will decrease quickly with temperature and may therefore be confirmed by the low-temperature studies.

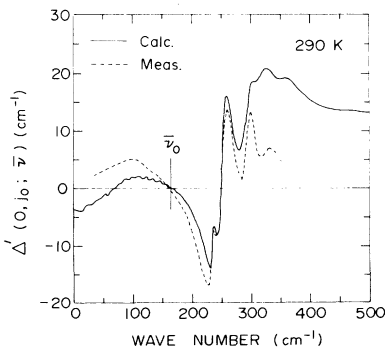

FIG. 10. Measured and calculated wave-number shift of the TO resonance in NaCl at 290 K. The prime on $\Delta'(0,j_0;\bar{\nu})$ indicates that the shift has been set to zero at the observed resonance wave number $\bar{\nu}_0$.

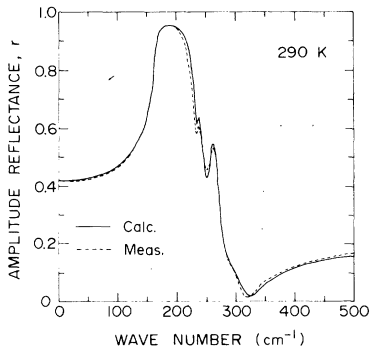

FIG. 11. Calculated and measured amplitude reflectance r of NaCl at 290 K. The power reflectivity $R = \hat{r}\hat{r}^*$, where $\hat{r} = re^{i\theta}$.

IV. OPTICAL PROPERTIES

In this section we are merely presenting the measured and calculated optical properties. The calculations all use the damping spectrum of Fig. 9 together with the wave-number shift calculated from the damping by means of a Kramers-Kronig procedure previously outlined.[1] This latter may be seen in Fig. 10 together with the spectrum obtained from the measurements. It may be seen from Eq. (5) that the optical properties are fairly insensitive to the wave-number shift except near $\bar{\nu}_0$, and so the measurements quickly become noisy away from $\bar{\nu}_0$. It is the damping spectrum which is important. The direct measurements were of reflectance amplitude and phase, as outlined in Sec. II and these may be seen in Figs. 11 and 12, respectively. The experimental error of the reflectance ranged from 0.2% at the maximum to 2% at the minimum and 4% at 500 cm^{-1}. The discrepancy just after 200 cm^{-1} in the damping of Fig. 9 shows up in both the reflectance and phase. The agreement in the remainder of these two figures is excellent. It should be noted that in all of the figures from Fig. 11 onwards, the measured properties are plotted all the way from 25 to 500 cm^{-1}. If the

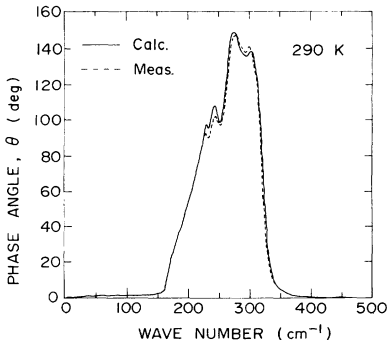

FIG. 12. Calculated and measured reflectance phase angle θ of NaCl at 290 K. See the caption for Fig. 11.

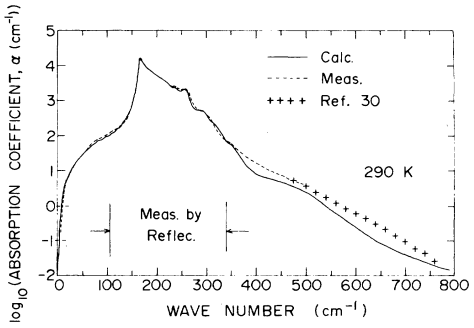

FIG. 13. Calculated and measured absorption coefficient α of NaCl at 290 K. The measurements below 110 cm^{-1} and above 340 cm^{-1} were from power-transmission experiments. Good overlap with the dispersive-reflection measurements was obtained. The crosses are from Harrington *et al.* (Ref. 30).

dashed line is not visible, it is because it completely overlaps the calculated full line. As mentioned in Sec. II the phase is noisy below 110 cm^{-1} and above 340 cm^{-1} so that direct absorption-coefficient measurements were performed in these regions. These are shown in Fig. 13 together with that obtained from the phase, and the measurements from Ref. 30. The discrepancy in Fig. 9 at 400 cm^{-1} is evident here together with the obvious need for higher-order processes beyond. For completeness the refractive index is shown in Fig. 14 and the real and imaginary dielectric constants in Figs. 15 and 16, respectively. We obtain $\bar{\nu}_{LO}$ equal to 265 ± 0.5 cm^{-1} as opposed to the neutron result[29] of 262 ± 7 cm^{-1}. Our agreement with the low-frequency real dielectric constant gives a value of 1.084 for the effective charge e^*.

V. CONCLUSION

It has long been recognized that asymmetric Fourier spectroscopy, or in our case dispersive-reflection spectroscopy, is the best means of ob-

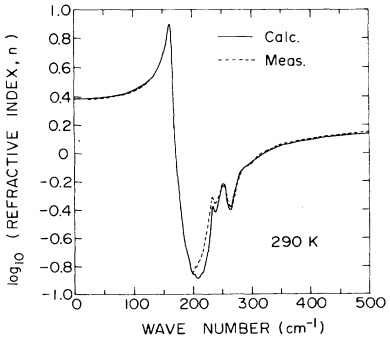

FIG. 14. Calculated and measured refractive index n of NaCl at 290 K. The discrepancy just after 200 cm^{-1} is again evident.

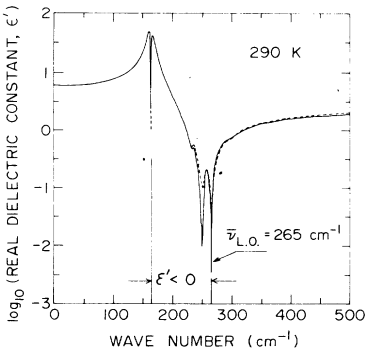

FIG. 15. Calculated and measured real part ϵ' of the dielectric constant of NaCl at 290 K.

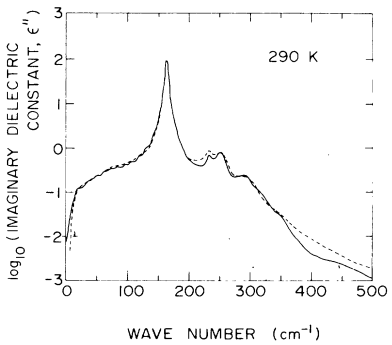

FIG. 16. Calculated and measured imaginary part ϵ'' of the dielectric constant of NaCl at 290 K.

taining far-infrared optical properties. It obviates the need for restrictive and sometimes inaccurate Kramers-Kronig analyses. The main difficulties associated with the asymmetric reflection method, namely, phase errors resulting from the exchange of sample surface with reference surface, and from the performance of separate runs on each, have been eliminated by aluminizing the sample in the manner described and alternately switching from sample to reference at each step of the micrometer drive. Very accurate data were quickly obtained by this method.

It has also been well recognized that quartic anharmonicity must be included in the room-temperature damping of the TO resonance in the alkali halides. This has been done by us for the first time in this study and the detailed form of the quartic-coupling coefficient that we derived has been presented. The strong role of the flat TO mode in this three-phonon damping has been observed. The advantage of obtaining good high-resolution experimental data throughout the spectrum is that the lifetime broadening of the two or three phonons to which the TO mode relaxes then becomes evident. This broadening can be determined from the experimental data and incorporated into the calculations. The end result is excellent overall agreement. The cause of the minor remaining discrepancies may be learned from future low-temperature studies.

---

*Work supported by Grant No. A5653 from the National Research Council of Canada.

[1]J. E. Eldridge and Roger Howard, Phys. Rev. B 7, 4652 (1973).
[2]K. W. Johnson and E. E. Bell, Phys. Rev. 187, 1044 (1969).
[3]K. Hisano, F. Placido, A. D. Bruce, and G. D. Holah, J. Phys. C 5, 2511 (1972).
[4]E. E. Bell, Infrared Phys. 6, 57 (1966); E. E. Russell and E. E. Bell, *ibid.* 6, 75 (1966).
[5]J. I. Berg and E. E. Bell, Phys. Rev. B 4, 3572 (1971).
[6]T. J. Parker, W. G. Chambers, and J. F. Angress, Infrared Phys. 14, 207 (1974).
[7]J. R. Birch, G. D. Price, and J. Chamberlain, Infrared Phys. 16, 311 (1976).
[8]J. Gast and L. Genzel, Opt. Commun. 8, 26 (1973).
[9]P. R. Staal and J. E. Eldridge, Infrared Phys. 17, 299 (1977).
[10]V. V. Mitskevich, Sov. Phys.-Solid State 3, 2211 (1962).
[11]R. A. Cowley, Adv. Phys. 12, 421 (1963).
[12]E. R. Cowley and R. A. Cowley, Proc. R. Soc. Lond. A 287, 259 (1965).
[13]E. R. Cowley, J. Phys. C 5, 1345 (1972).
[14]A. D. Bruce, J. Phys. C 6, 174 (1973).
[15]A. A. Maradudin and A. E. Fein, Phys. Rev. 128, 2589 (1962).
[16]R. F. Wallis, I. P. Ipatova, and A. A. Maradudin, Sov. Phys.-Solid State 8, 850 (1966).
[17]I. P. Ipatova, A. A. Maradudin, and R. F. Wallis, Phys. Rev. 155, 882 (1967).
[18]R. P. Lowndes, Phys. Rev. B 6, 1490 (1972).
[19]A. Rastogi, J. P. Hawranek, and R. P. Lowndes, Phys. Rev. B 9, 1938 (1974).
[20]J. E. Eldridge, Phys. Rev. B 6, 1510 (1972).
[21]J. E. Eldridge and K. A. Kembry, Phys. Rev. B 8, 746 (1973).
[22]J. A. B. Beairsto and J. E. Eldridge, Can. J. Phys. 51, 2550 (1973).
[23]J. E. Eldridge, Roger Howard, and P. R. Staal, Can. J. Phys. 55, 227 (1977).
[24]Neglect of this contribution to the damping is the cause of the low-temperature disagreement between experiment and theory in Ref. 19.
[25]R. B. Barnes and M. Czerny, Phys. Rev. 38, 338 (1931).
[26]R. P. Lowndes and D. H. Martin, Proc. R. Soc. A 308, 473 (1969).
[27]A. M. Karo and J. R. Hardy, Phys. Rev. 129, 2024 (1963).
[28]F. G. Fumi and M. P. Tosi, J. Phys. Chem. Solids 25, 31 (1964).

[29]R. E. Schmunk and D. R. Winder, J. Phys. Chem. Solids 31, 131 (1970).
[30]J. A. Harrington, C. J. Duthler, F. W. Patten, and M. Hass, Solid State Commun. 18, 1043 (1976).
[31]A. D. Bruce, J. Phys. C 5, 2909 (1972).
[32]C. J. Duthler and M. Sparks, Phys. Rev. B 9, 830 (1974).
[33]C. J. Duthler, Phys. Rev. B 14, 4606 (1976).
[34]J. E. Eldridge and P. R. Staal, Phys. Rev. B (to be published).
[35]K. Fischer, Phys. Status Solidi B 66, 449 (1974).